Research article

LUMINESCENCE
The Journal of Biological and Chemical Luminescence

Received: 23 August 2015, Revised: 19 September 2015, Accepted: 23 September 2015 Published online in Wiley Online Library: 5 November 2015

(wileyonlinelibrary.com) DOI 10.1002/bio.3053

Application of a fluorescent biosensor based-on magneto-γ-Fe_2O_3–methyldopa nanoparticles for adsorption of human serum albumin

Nahid Shahabadi,[a,b]* Maryam Maghsudi[a] and Farshad Shiri[a]

ABSTRACT: Understanding and controlling the interaction between the polymer methyldopa (2-amino-3-(3,4-dihydroxyphenyl)-2-methyl-propanoic acid) (PMDP)–γ-Fe_2O_3 nanoparticles and biological fluids is important if the potential of nanoparticles (NPs) in biomedicine is to be realized. Physicochemical studies on the interactions between proteins and NPs are influenced by the surface properties of the NPs. To identify the effects of the NP surface, interactions between human serum albumin (HSA) and PMDP–γ-Fe_2O_3 NPs were investigated. Here, the adsorption of HSA onto small (10–30 nm diameter) PMDP–γ-Fe_2O_3 NPs was quantitatively analyzed using spectroscopic methods. The fluorescence quenching data were checked for the inner-filter effect, the main confounding factor in the observed quenching. The binding constants, K_a, were calculated at different temperatures, using a nonlinear fit to the experimental data, and the thermodynamic parameters ΔH, ΔS and ΔG were given. The obtained thermodynamic signature suggests that hydrophobic interactions at least are present. This result indicates that the structure of the protein turns from a structureless denatured state at pH 3 into an ordered biologically active native state on addition of PMDP–γ-Fe_2O_3 NPs. Copyright © 2015 John Wiley & Sons, Ltd.

Keywords: fluorescent biosensor; human serum albumin; adsorption; nanoparticles; spectroscopic techniques; inner-filter effect

Introduction

Interactions between nanoparticles (NPs) and proteins are a highly relevant in the medical application of nanomaterials (1,2). Various albumin proteins present in the bloodstream play a key role in the transportation of these NPs to their desired destination and any adverse modification of the protein conformation or functionality would consequently restrict their applicability.

Recently, there has been burgeoning research interest into protein–NP interactions using various combinations of NP and protein (3,4). Upon incorporation into the body, NPs are exposed to biological fluids such as lung epithelial lining fluid or blood plasma, which contain a variety of dissolved molecules, particularly proteins, and it is the NP–protein complexes rather than the NPs alone that determine the resulting biological responses (5). Understanding the nature of interactions (e.g. interaction forces, binding sites and affinity) and their subsequent effects (e.g. conformation and activity of the interacting proteins, stability and functionality of the NPs) are crucial for the better design and handling of nanomaterials in a biological environment.

By comparison, studies on the colloidal dispersion of bare NPs in these fields have been rare to date (6–8). Serum albumins, which have been widely used as model proteins in biophysical studies to address interactions with various ligands (9–12), belong to the class of transport proteins. Thus, an understanding of the possible interactions between NPs and serum proteins is essential in order to develop safe, engineered bio-nanomaterials. The interaction between an administered material and the plasma protein in the circulatory system govern the pharmacological behavior of the material within the body (13,14). Therefore, the use of serum albumins as an ideal counterpart in protein–NP interactions has attracted much attention in recent years.

At present, there are many reports for the determination of biomolecules, such as IgE (15), myoglobin (16), dopamine (17), C-reactive protein (18), procaterol hydrochloride (19), cefditoren pivoxil (20), nicotinamide (21) by using analytical methods. Quantification of albumin is clinically important, as it has been found to be an effective prognostic indicator. Human serum albumin (HSA) levels are typically ~ 50 g/L (~0.75 mM) for healthy individuals and low HSA concentrations (<1 g/L) indicate analbuminemia, a rare congenital disorder (22). Quantifying HSA, especially at low concentrations, is of great significance.

In this study, HSA was employed as a model transport protein to decipher its interactions with a magnetic NP of PMDP–γ-Fe_2O_3. The interaction of HSA with the PMDP–γ-Fe_2O_3 NPs was monitored by following modifications in the intrinsic fluorescence properties of the protein using a constant protein concentration and different concentrations of nanoparticles. Information regarding quenching mechanisms, binding parameters, thermodynamic parameters, binding mode and affinity, and conformation changes are reported in this work.

* Correspondence to: N. Shahabadi, Department of Inorganic Chemistry, Faculty of Chemistry, Razi University, Kermanshah, Iran. Tel/Fax: +98-83-34274559. E-mail: nahidshahabadi@yahoo.com

[a] Department of Inorganic Chemistry, Faculty of Chemistry, Razi University, Kermanshah, Iran

[b] Medical Biology Research Center (MBRC), Kermanshah University of Medical Sciences, Kermanshah, Iran

Experimental

Reagents

HSA (>96%, essentially fatty acid free, lyophilized powder) was purchased from Sigma (St Louis, MO, USA). HSA solution was prepared in 0.001 M sodium phosphate buffer (pH 7.4) and was kept in the dark at 4°C and used soon after. All other chemicals were of analytical grade and were used without further purification.

Methods

Absorption spectroscopy

The absorption spectra were recorded on an UV Win T80 spectrophotometer. Quartz cuvettes of 1 cm were used and the absorption spectra were recorded for free HSA (50 μg/mL) and for its PMDP–γ-Fe_2O_3 NPs (0.06–2 μg/mL).

Fluorescence spectroscopy

In each assay, a 2.0 mL sample containing (10 μg/mL) HSA was added to a 1 cm quartz cuvette and then titrated by stepwise addition of small aliquots (μL) of a 0.1 mg/mL PMDP–γ-Fe_2O_3 NPs stock solution at 5-min intervals. The fluorescence emission spectra of HSA were recorded from 300 to 450 nm on a FP-6200 spectrofluorimeter (JASCO, Japan, Tokyo) at a λ_{ex} of 295 nm with excitation and emission slits at 5 and 10 nm.

Results and discussion

Synthesis and characterization of PMDP–γ-Fe_2O_3 NPs

The NP used in this study was synthesized in the form of PMDP–γ-Fe_2O_3 NPs (stable colloidal suspension) as described previously (23). The stability of the as-prepared colloidal suspension was adjudged on the basis of the zeta potential obtained from dynamic light scattering experiments. The analysis suggests that the particles are negatively charged over the entire pH range and thus well stabilized in the aqueous medium through electrostatic repulsion.

Fourier transform infrared (FTIR) spectra were used to demonstrate the successful methyl dopa (MDP) ligand exchange onto PMDP–γ-Fe_2O_3 magnetic nanoparticles (Fig. 1A). The FTIR spectrum of freeze-dried initial PMDP–γ-Fe_2O_3 (Fig. 1A) verifies the presence of the maghemite phase of iron oxide. The results clearly indicate the presence of a polymerized aromatic structure and thus PMDP coating of MNPs was successfully carried out. Transmission electron microscopy (TEM) analysis was performed to give an idea of the size, shape and distribution of the NPs in solution. The observations are shown in Fig. 1(B). The particles were found to be almost uniform in size and spherical in shape with an average diameter of 30 nm. The TEM image (label B in Fig. 1B) also indicates that the sample is composed of core–shell nanocrystals. More details about MDP–γ-Fe_2O_3 are given in our recent study (23).

Interactions between PMDP–γ-Fe_2O_3 NPs and HSA

Given that metallic NPs quench molecular fluorescence within 10 nm of their surface, fluorescence quenching experiments can be used to quantify the adsorption of fluorescent proteins to PMDP–γ-Fe_2O_3 NPs (24). It is assumed that the adsorption of proteins onto NPs quenches the protein fluorescence (25,26). By titrating PMDP–γ-Fe_2O_3 NPs into a HSA solution, the decrease in the fluorescence intensity of HSA with respect to the concentration of PMDP–γ-Fe_2O_3 NPs can be tabulated and quantified (Fig. 2).

To investigate the selectivity of the proposed method toward HSA, interference experiments were performed. The study was carried out using the fluorescence method in the presence of 5 μg/mL HSA and various quantities of potential interfering substances at pH 7.0. The results suggest that a 15-fold excess of insulin, 20-fold excess of proteinase K and 20-fold excesses of Phe, Gly, Ala and Arg have no influence on the signals of PMDP–γ-Fe_2O_3 with deviations of $< 5\%$. However, a sixfold excess of calf thymus deoxy ribonucleic acid (ct-DNA) interfered with the determination of HSA. BSA was also studied, because its structure is very similar to that of the target analyte. The results indicated that a twofold excess of BSA can influence the peak intensity and current response of HSA.

In the case of fluorescence quenching titrations, the high absorbance of PMDP–γ-Fe_2O_3 nanoparticles can trivially absorb protein fluorescence even when the proteins are not closely bound to the surface. At higher concentrations of PMDP–γ-Fe_2O_3 NPs, the presence of the PMDP–γ-Fe_2O_3 NP metal core can scatter the input and output fluorescence, further reducing the fluorescence signal. These effects, which are called the inner-filter effect (IFE), act together to produce a fluorescence quenching curve that is not representative of the actual binding of proteins to PMDP–γ-Fe_2O_3 NPs.

It should be noted that, as the concentrations of PMDP–γ-Fe_2O_3 NPs increased, an instrumental IFE caused a slight decrease in the fluorescence emission intensity (27). This effect is an inherent problem of many fluorimetric procedures, leads to results that depart from the initial linearity and must be taken into account.

In this study, we eliminated the IFE for all of the fluorescence results to obtain accurate data. To eliminate the IFE of HSA and PMDP–γ-Fe_2O_3 NPs, absorbance measurements were performed at the excitation and emission wavelengths of the fluorescence measurements. The fluorescence intensity was corrected using equation (1) (27):

$$F_{cor} = F_{obs} 10^{(A_1 + A_2)/2} \quad (1)$$

Where F_{cor} and F_{obs} are the corrected and observed fluorescence intensity, respectively, and A_1 and A_2 are the sum of the absorbance of HSA and PMDP–γ-Fe_2O_3 NPs at the excitation and emission wavelengths, respectively. Using equation (1), we calculated F_{cor} for each measured fluorescence spectrum. The IFE are depicted in Fig. 3(A,B).

To determine the mode of binding between HSA and PMDP–γ-Fe_2O_3 NPs, fluorescence intensity data at different temperatures were analyzed using the Stern–Volmer equation (equation (2)):

$$\frac{F_0}{F} = 1 + K_{SV}[Q] \quad (2)$$

Where F_0 and F are the fluorescence intensities in the absence and presence of PMDP–γ-Fe_2O_3 NPs, K_{SV} (M = g/mL) is the Stern–Volmer quenching constant and [*Q*] is the concentration of PMDP–γ-Fe_2O_3 NPs (g/mL). If the resulting plots exhibit a good linear relationship, this is generally indicative of a purely collisional or static quenching process

LUMINESCENCE
The Journal of Biological and Chemical Luminescence

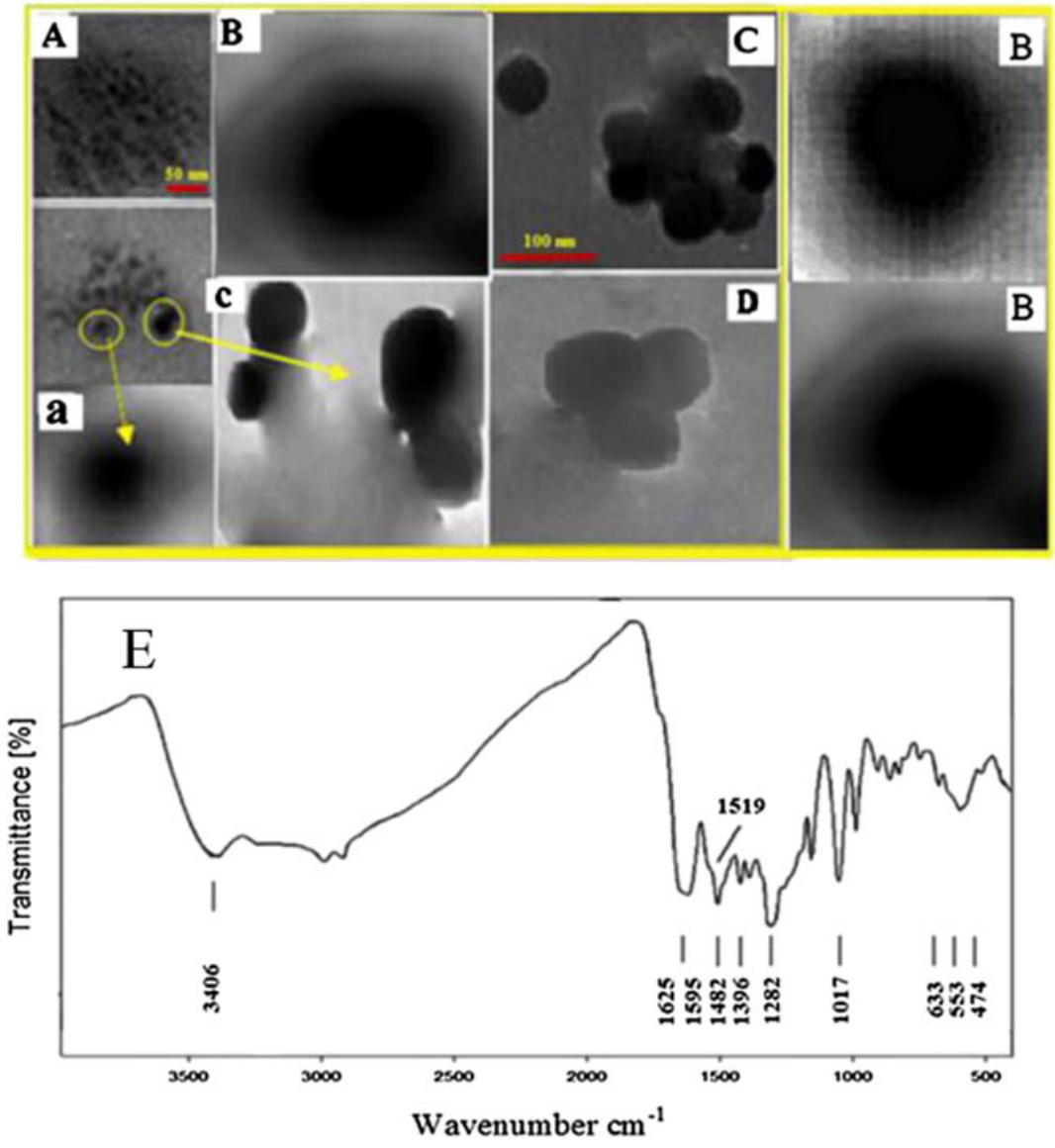

Figure 1. A) TEM image immediately after drying and (a) presence of a "cloudy" region around the particles (B) typical core-shell structure of a MDP–γ-Fe $_2O_3$ (C, c) TEM image after 30 min drying (D) aggregation/coalescence. E) FT-IR spectrum of PMDP–γ-Fe_2O_3 NPs recorded between 4000 and 400 cm

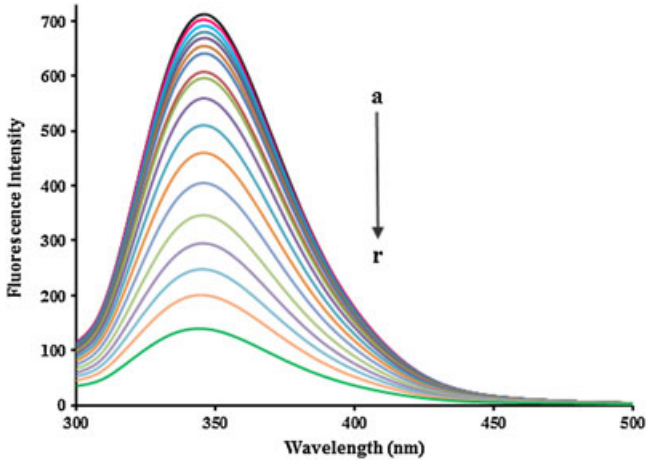

Figure 2. The quenching effect of PMDP–γ-Fe_2O_3 NPs on HSA fluorescence. (a–r) HSA, 10 μg/mL; PMDP–γ-Fe_2O_3, 0.02, 0.06, 0.2, 0.6, 0.8, 1.4, 1.6, 1.8, 2, 4, 6, 8, 12, 14, 16, 20 and 40 μg/mL.

(28). However, the Stern–Volmer plot showed a major positive deviation (Fig. 3C), indicating the presence of both static and dynamic quenching. Therefore, the data were processed based on a modified Stern–Volmer equation:

$$\frac{F_0}{F} = 1 + K_{SV}[Q]\exp(V[Q]\}) \quad (3)$$

Where V is the static quenching constant, the value of which can be obtained from equation (3) by plotting against [Q] and varying V until a linear plot is acquired (Fig. 3D). K_{SV} can then be obtained from the slope of the plot. The values of V and K_{SV} at different temperatures (288, 298 and 310 K) are presented in Table 1. It is seen that K_{SV} increases as the temperature increases, indicating that the quenching mechanism may be dynamic quenching, although static quenching makes a small contribution as seen from the positive deviation in the Stern–Volmer plot.

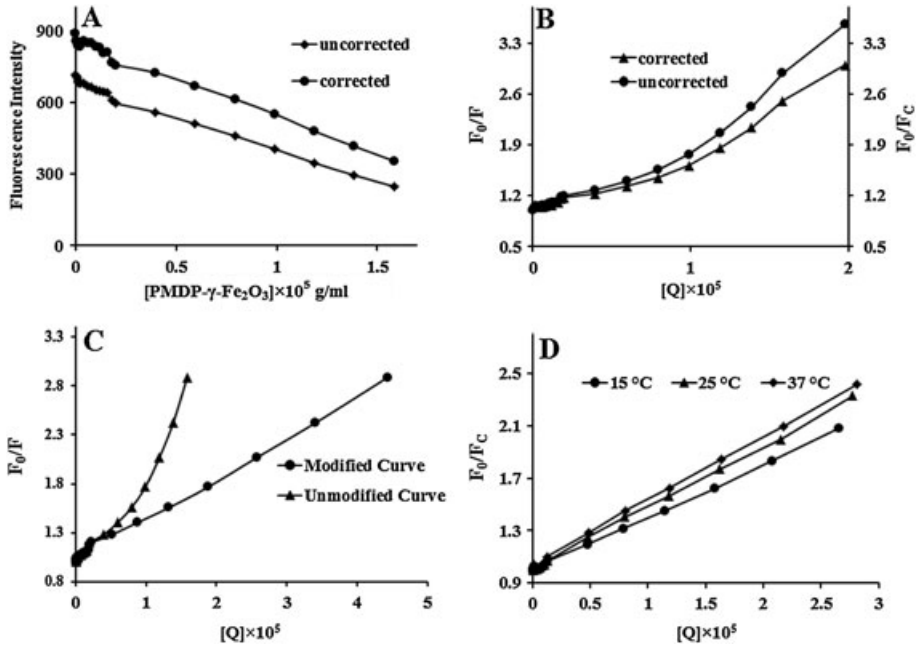

Figure 3. (A) Fluorescence quenching titrations of HSA in the presence of PMDP–γ-Fe_2O_3 NPs before (♦) and after (●) correction at 25°C. (B) Data points from fluorescence quenching titrations before (●) and after (◄) correction using the Stern–Volmer relationship. The left axis (F_0/F) corresponds to the uncorrected fluorescence data, whereas the right axis (F_0/F_C) corresponds to the IFE-corrected data at 25°C. (C) Modified and unmodified Stern–Volmer plots of the interaction of PMDP–γ-Fe_2O_3 NPs with HSA at 25°C. (D) Modified Stern–Volmer plot for the quenching of HSA fluorescence by PMDP–γ-Fe_2O_3 NPs at three temperatures: 25, 37 and 47°C.

Table 1. The binding parameters of PMDP–γ-Fe_2O_3 NPs with HSA at different temperatures

T (K)	$10^{-4} \times K_{SV}$ (M)	$10^{-4} \times V$ (M)	K_d (μg/mL)	F_c (a.u.)	Adj. R^2
288	4.03	4.70	9.71	0.06	0.9872
298	4.72	4.80	8.06	0.14	0.9841
310	5.08	4.90	6.14	30	0.9830

Determination of the binding stoichiometry

An important element in the study of the HSA–PMDP–γ-Fe_2O_3 NPs interaction is the binding stoichiometry of the reactants. Job's plot analysis (known as the method of continuous variation) is very useful in characterizing the complex formed by the interaction of the two species. In the continuous variation method, the total molar concentration, C_0 (g/mL) = [HSA] + [PMDP–γ-Fe_2O_3 NPs], is held constant, but the mole fractions χ are varied. The binding stoichiometry is calculated from the mole fraction of HSA or PMDP–γ-Fe_2O_3 NPs at a specific point (29).

The mole fraction χ of HSA at the maximum of the Job's curve is $\chi = [HSA]/C_0 = (n + 1)^{-1}$, where n is the number of binding sites on HSA, only if C_0 is sufficiently high relative to the dissociation constant K_d. The recommended concentration of C_0 is at least five times greater than the value of K_d. Taking into account the K_d values determined by equilibrium dialysis and fluorescence spectroscopy (30,31), Job's plot analyses were performed at C_0 = 10, 50 and 80 μg/mL. The obtained results (Fig. 4A) show that the maximum of the Job's curve occurs at χ = 0.5, indicating the existence of a complex with a 1:1 stoichiometry within the range of the investigated concentrations.

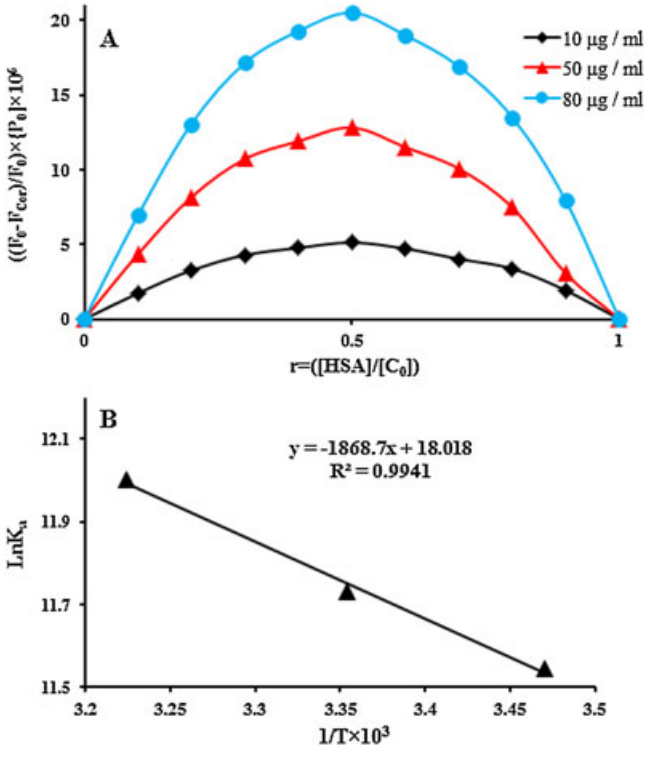

Figure 4. (A) Job's plots of HSA–PMDP–γ-Fe_2O_3 NP fluorescence at a total concentration C_0 of 10, 50 and 80 μg/mL. (B) Van't Hoff plot of the interaction of PMDP–γ-Fe_2O_3 NPs and HSA.

Determination of the binding constant

Many different equations are used to analyze quenching data (32), and we used the most generally valid to analyze fluorescence

LUMINESCENCE
The Journal of Biological and Chemical Luminescence

changes upon formation of a 1:1 complex (33), which in the normalized version can be expressed as:

$$\frac{F_0 - F_{corr}}{F_0 - F_C} = \frac{[P]_t + [L]_a + K_d - \sqrt{([P]_t + [L]_a + K_d)^2 - 4[P]_t[L]_a}}{2[P]_t} \quad (4)$$

Where F_{corr} is the measured fluorescence corrected for the IFE, F_0 is the fluorescence in the absence of PMDP–γ-Fe_2O_3 NPs, F_C is the fluorescence of the fully complexed HSA, K_d is the dissociation constant, $[P]_t$ is the concentration of HSA (g/mL), and $[L]$ is the concentration of added PMDP–γ-Fe_2O_3 NPs (g/mL). The values of K_d and F_C were obtained for different temperatures by fitting the experimental data to equation (4). The obtained results are presented in Table 1.

Force acting between PMDP–γ-Fe_2O_3 NPs and HSA

Fluorescence is widely used in studying the mode of interaction between a biosystem and drug molecules. Ross and Subramanian summarized the thermodynamic law judging the primary binding driving force between biomacromolecules and drugs: (1) $\Delta H > 0$ and $\Delta S > 0$ indicate a hydrophobic interaction; (2) $\Delta H < 0$ and $\Delta S < 0$ suggest that hydrogen bonds and van der Waal's force dominate; and (3) $\Delta H \sim 0$ and $\Delta S > 0$ imply that electrostatic interactions are dominant (34).

The values of ΔH and ΔS can be estimated from the van't Hoff equation (equation (5)):

$$lnK = -\frac{\Delta H}{RT} + \frac{\Delta S}{R} \quad (5)$$

Where K is analogous to the effective quenching constant K_a at the same temperature and R is the gas constant. It can be seen from Fig. 4(B) that there is a good linear relationship between ln$K$ and 1/T, which means that the enthalpy change (ΔH) is constant across the range of temperatures discussed. ΔH could be measured from the slope of the van't Hoff plot, whereas the entropy change (ΔS) can be obtained from the intercept.

Detailed data are given in Table 2. The obtained values of $\Delta H > 0$ and $\Delta S > 0$ suggest that the driving force of this process is mainly typical hydrophobic interactions, and hydrogen bonds and van der Waal's force are not dominant. The value of ΔG at different temperatures can be calculated according to equation (6):

$$\Delta G = \Delta H - T\Delta S \quad (6)$$

Because this quenching is spontaneous, the Gibbs' free energy of this process is negative ($\Delta G < 0$). Accordingly, the entropy change of the system is absolutely positive ($\Delta S > 0$). Therefore, PMDP–γ-Fe_2O_3 NP-induced quenching of HSA fluorescence is an entropy-driven spontaneous process based on the above analysis; however, the change in enthalpy is detrimental to the spontaneous process. The values of the thermodynamic parameters K_a, ΔS, ΔH and ΔG are given in Table 2.

Table 2. Binding constants (K_b) and relative thermodynamic parameters of the HSA–PMDP–γ-Fe_2O_3 NPs system at different temperatures

T (K)	$10^{-5} \times K_b$ (M)	ΔH (kJ/mol)	ΔS (J/mol/K)	ΔG (kJ/mol)
288	1.03 ± 0.02			−27.63 ± 0.02
298	1.24 ± 0.02	15.54 ± 0.01	149.80 ± 0.04	−29.13 ± 0.02
310	1.63 ± 0.02			−30.92 ± 0.02

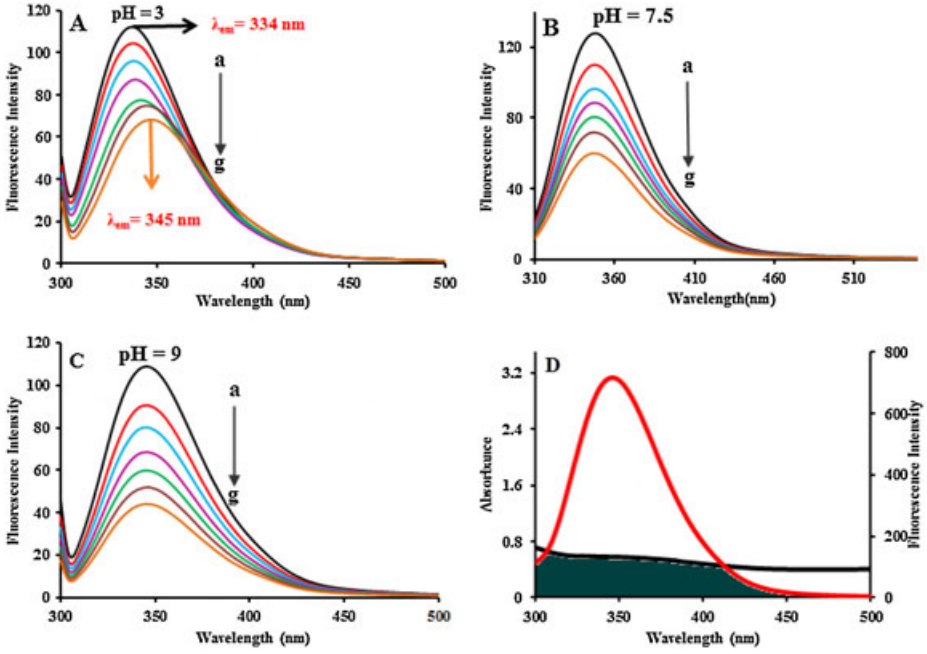

Figure 5. (A–C) Fluorescence-induced HSA by PMDP–γ-Fe_2O_3 NPs at different pH values using fluorescence spectroscopy. (a–g) HSA, 10 μg/mL; PMDP–γ-Fe_2O_3, 1.5, 3, 4.3, 5.7, 7 and 10.3 μg/mL. (D) Spectral overlap between the fluorescence emission spectrum of HSA (red line) and the absorption spectrum of PMDP–γ-Fe_2O_3 NPs (black line) in 100 mM phosphate buffer pH 7.5, λ_{ex} = 295 nm; λ_{em} = 347 nm.

Effect of pH

These observations suggest that the binding process is pH independent, and negatively charged proteins are required for adsorption with PMDP–γ-Fe_2O_3 NPs. Such quantitative pictures of the adsorption-induced HSA allow us to study the effects of different environmental conditions on the adsorption process. We first study the adsorption induced HSA by PMDP–γ-Fe_2O_3 NPs at different pH values using fluorescence spectroscopy (Fig. 5A–C). The isoelectric point of HSA is 4.7. Therefore, it is slightly negatively charged at pH 7.5, highly negatively charged at pH 9, and positively charged at pH 3. The effects of electrostatic interactions on the adsorption of HSA on PMDP–γ-Fe_2O_3 NP surfaces are not apparent. This is consistent with our conclusion that hydrophobic interactions between proteins and NPs are the driving forces behind the induced adsorption. These results suggest that the structure of PMDP–γ-Fe_2O_3 NPs and HSA protein remain the same and the degree of interaction between them did not change with the pH. At physiological pH (7.4), HSA assumes the native form (N), which changes to a fast migrating form (F) at pH $<$ 4.3, and at pH $<$ 2.7 changes to the fully extended form (E). By contrast, on the basic side at pH $>$ 8 the 'N' form changes to the basic form (B) (35).

The emission peaks for pH 3.0 (F, fast migrating form), pH 7.5 (N, native form) and pH 9.0 (B, basic form) are at 334, 345 and 354 nm respectively, indicating different conformational states of HSA. From the emission spectra of PMDP–γ-Fe_2O_3 NPs, it is clear that the fluorescence due to tryptophan was drastically quenched in the presence of PMDP–γ-Fe_2O_3 NPs at three mentioned pH. The observed quenching of photoluminescence intensities for the F, N and B forms of human serum albumin are 46% with a red shift of 12 nm, 53% and 60%, respectively (36). This indicates a change in the structure of the protein from a structureless denatured state at pH 3 to an ordered biologically active native state on addition of PMDP–γ-Fe_2O_3 NPs (Scheme 1).

To further investigate whether electrostatic interactions play a role in protein–PMDP–γ-Fe_2O_3 NPs, we adjusted the ionic strength of the assembly solution by adding NaCl (0−0.015 M).

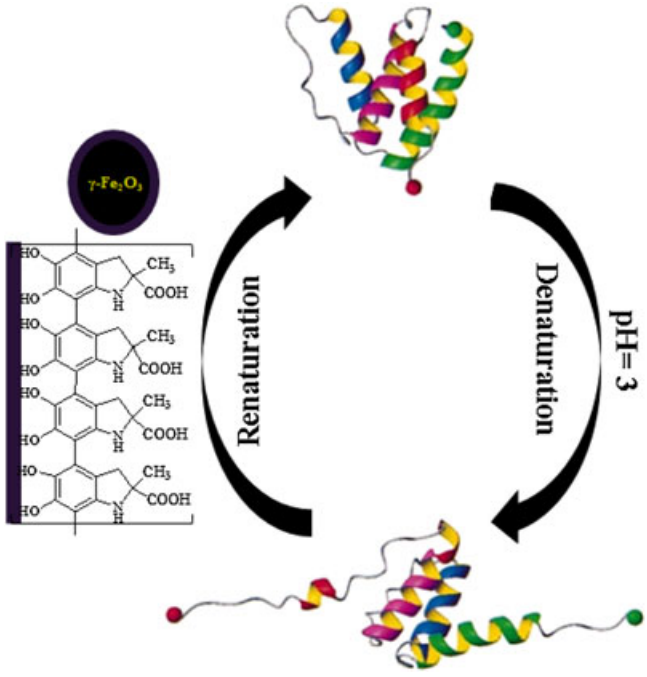

Scheme 1. Schematic protein folding in the presence of PMDP–γ-Fe_2O_3 NPs.

Effect of ionic strength

Because the foregoing discussion reveals a role for electrostatic forces in the HSA–PMDP–γ-Fe_2O_3 NPs interaction, the effect of ionic strength was studied. Here, we explore the effect of increasing ionic strength of the medium (increasing concentration of NaCl) on the intrinsic fluorescence of the protein and protein–PMDP–γ-Fe_2O_3 NPs systems individually.

The PMDP–γ-Fe_2O_3 NPs that we used in this study have negative and slightly positive charges under these conditions (PBS buffer), as confirmed by their zeta potentials (Fig. 5C). The adsorption of HSA on the PMDP–γ-Fe_2O_3 NPs surface was also changed slightly by the ionic strength, further confirming that electrostatic interactions play only minor roles in the process (Fig. 6A).

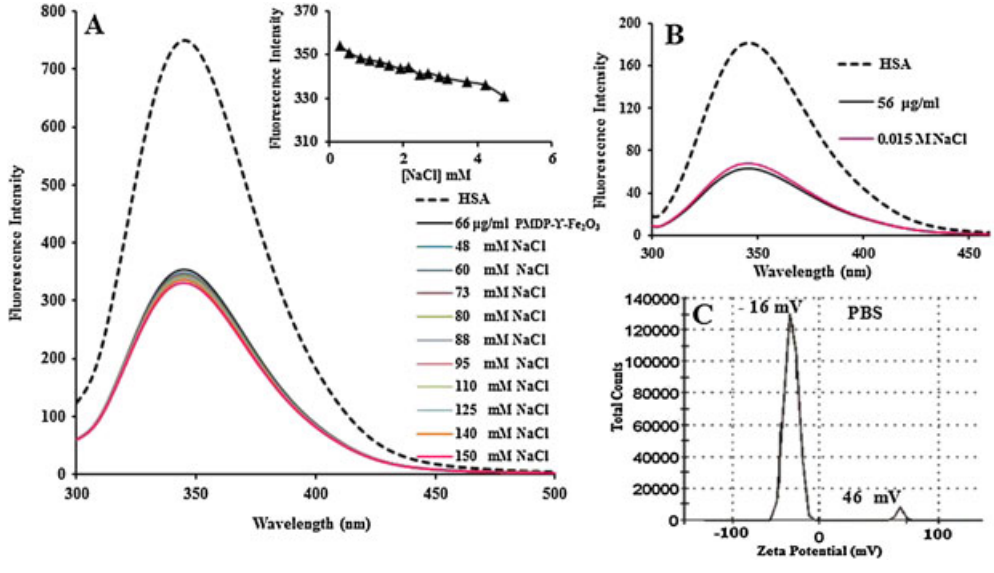

Figure 6. (A,B) Adsorption of HSA on the surface of PMDP–γ-Fe_2O_3 NPs at different ionic strengths. (C) Zeta-potential of PMDP–γ-Fe_2O_3 dispersions in Phosphate Buffered Saline (PBS).

LUMINESCENCE
The Journal of Biological and Chemical Luminescence

Energy transfer between PMDP–γ-Fe_2O_3 NPs and HSA

Energy transfer between drugs and HSA usually can be divided into two types, radiative and nonradiative. The latter can be explained and determined by Förster's resonance energy transfer theory (FRET). Förster's theory is often used to determine the distance between the amino acid residues and the drug at the binding site. This can be estimated by calculating the overlap of the fluorescence spectra of HSA and the UV–vis spectra of the drug (37).

According to Förster's theory, the efficiency of the energy transfer between the donor and acceptor, E, can be calculated using equation (7) (38):

$$E = 1 - \frac{F}{F_0} = \frac{R_0^6}{(R_0^6 + r^6)} \quad (7)$$

Where r is the distance between the donor and the acceptor and R_0 represents the critical distance when the transfer efficiency is 50%. R_0 can be calculated using equation (8):

$$R_0^6 = 8.8\times10^{-25}K^2N^{-4}\Phi J \quad (8)$$

Where K^2 is the orientation factor involving the geometry of the donor–acceptor dipole, N is the refractive index of the medium, Φ is the donor's fluorescence quantum yield, and J expresses the degree of spectral overlap between the donor's emission and acceptor's absorption. J is usually calculated using equation (9):

$$J = \frac{\Sigma F(\lambda)\varepsilon(\lambda)\lambda^4\Delta\lambda}{\Sigma F(\lambda)\Delta\lambda} \quad (9)$$

Where $F(\lambda)$ is the fluorescence intensity of the donor at wavelength λ and is dimensionless, $\varepsilon(\lambda)$ is the molar absorption coefficient of the acceptor at wavelength λ.

We can evaluate J by integrating the overlap spectra in Fig. 6(D) according to equation (9). According to equations (7)–(9) and using $K^2 = 2/3$, $n = 1.336$ and $\Phi = 0.15$ (39), the following data are obtained: $J = 2.84 \times 10^{-16}$ cm^3/L/mol, $R_0 = 5.35$ nm, $E = 0.8$ and $r = 4.09$ nm. The value of r is in the range of 2–8 nm, this only means it is possible Electron Transfer (ET) occurs between PMDP–γ-Fe_2O_3 NPs and HSA.

UV–vis absorption spectral studies

UV–vis absorption spectroscopy is a simple but effective method for detecting conformational changes in proteins and during ligand–protein complex formation. Difference absorption spectra for HSA with various quantities of PMDP–γ-Fe_2O_3 NPs were obtained by subtracting the corresponding spectrum for free PMDP–γ-Fe_2O_3 NPs from those for the PMDP–γ-Fe_2O_3 NPs–HSA complex (Fig. 7). On gradual addition of PMDP–γ-Fe_2O_3 NPs to HSA solution, the intensity of the peak at 279 nm increases, which indicates the formation of a complex between HSA and PMDP–γ-Fe_2O_3 NPs and a change in the protein conformation (40).

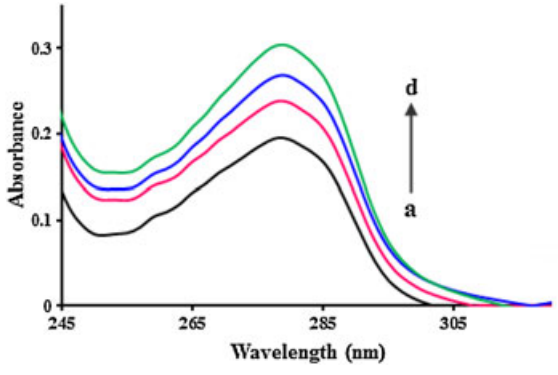

Figure 7. UV–vis absorption spectra of HSA (a: 50 μg/mL,) with various concentrations of PMDP–γ-Fe_2O_3 NPs. (b–d) 0.06, 0.15 and 2 μg/mL.

Conclusions

In summary, the adsorption of HSA onto PMDP–γ-Fe_2O_3 NPs was studied using a combination of UV–vis spectroscopy and fluorescence quenching. The results showed different protein adsorption behaviors depending on the composition and structure of the NP surface ligand. This study also demonstrated that the NP surface could be a tunable property in NP design for specific applications. Thermodynamic parameters revealed that the protein–NP interaction process is entropy driven ($\Delta S > 0$), being caused by the release of a large amount of water from the environment surrounding of the hydrophobic region of PMDP–γ-Fe_2O_3 NPs.

Acknowledgments

Financial support from the Razi University Research Center and Medical Biology Research Center (MBRC) Kermanshah University of Medical Sciences is gratefully acknowledged.

References

1. Koegler P, Clayton A, Thissen H, Santos GNC, Kingshott P. The influence of nanostructured materials on biointerfacial interactions. Adv Drug Deliv Rev 2012;64:1820–39.
2. Nel A, Madler EL, Velegol D, Xia T, Hoek EMV, Somasundaran P, et al. Understanding biophysicochemical interactions at the nano–bio interface. Nat Mater 2009;8:543–57.
3. Schlorf T, Meincke M, Kossel E, Gluer CC, Jansen O, Mentlein R. Biological properties of iron oxide nanoparticles for cellular and molecular magnetic resonance imaging. Int J Mol Sci 2010;12:12–23.
4. Liu S, Han Y, Qiao R, Zeng J, Jia Q, Wang Y, et al. Investigations on the interactions between plasma proteins and magnetic iron oxide nanoparticles with different surface modifications. J Phys Chem C 2010;114:21270–6.
5. Lynch I, Cedervall T, Lundqvist M, Cabaleiro-Lago C, Linse S, Dawson KA. The nanoparticle–protein complex as a biological entity; a complex fluids and surface science challenge for the 21st century. Adv Colloid Interface 2007;134–5:167–74.
6. Sun C, Fang C, Stephen Z, Veiseh O, Hansen S, Lee D, et al. Tumor-targeted drug delivery and MRI contrast enhancement by chlorotoxin-conjugated iron oxide nanoparticles. Nanomedicine 2008;3:495–505.
7. Milani S, Bombelli FB, Pitek AS, Dawson KA, Radler J. Reversible versus irreversible binding of transferrin to polystyrene nanoparticles: soft and hard corona. ACS Nano 2012;6:2532–41.
8. De M, You CC, Srivastava S, Rotello VM. Biomimetic interactions of proteins with functionalized nanoparticles: a thermodynamic study. J Am Chem Soc 2007;129:10747–53.
9. Tedesco AC, Oliveria DM, Lacava ZGM, Azevedo RB, Lima ECD, Gansau C, et al. Determination of binding constant K_b of biocompatible, ferrite-based magnetic fluids to serum albumin. J Appl Phys 2003;93:6704–6.
10. Yang Q, Liang J, Han H. Probing the interaction of magnetic iron oxide nanoparticles with bovine serum albumin by spectroscopic techniques. J Phys Chem B 2009;113:10454–8.
11. Shang W, Nuffer JH, Dordick JS, Siegel RW. Unfolding of ribonuclease A on silica nanoparticle surfaces. Nano Lett 2007;7:1991–5.
12. Paul B, Samanta KA, Guchhait N. Exploring hydrophobic subdomain IIA of the protein bovine serum albumin in the native, intermediate,

unfolded, and refolded states by a small fluorescence molecular reporter. J Phys Chem B 2010;114:6183–96.
13. Jisha VS, Arun KT, Hariharan M, Ramaiah D. Site-selective binding and dual mode recognition of serum albumin by a squaraine dye. J Am Chem Soc 2006;128:6024–5.
14. Banerjee T, Singh SK, Kishore N. Binding of naproxen and amitriltyline to bovine serum albumin: biophysical aspects. J Phys Chem B 2006;110:24147–56.
15. Jiang B, Li F, Yang C, Xie J, Xiang Y, Yuan R. Aptamer pseudoknot-functionalized electronic sensor for reagentless and single-step detection of immunoglobulin E in human serum. Anal Chem 2015;87:3094–8.
16. Kim D-H, Seo S-M, Cho H-M, Hong S-J, Lim D-S, Paek S-H. Continuous immunosensing of myoglobin in human serum as potential companion diagnostics technique. Biosens Bioelectron 2014;62:234–41.
17. Huang Q, Lin X, Lin C, Zhang Y, Hu S, Wei C. A high performance electrochemical biosensor based on Cu_2O–carbon dots for selective and sensitive determination of dopamine in human serum. RSC Adv 2015;5:54102–8.
18. Kokkinos C, Prodromidis M, Economou A, Petrou P, Kakabakos S. Disposable integrated bismuth citrate-modified screen-printed immunosensor for ultrasensitive quantum dot-based electrochemical assay of C-reactive protein in human serum. Anal Chim Acta 2015;886:29–36.
19. Liu J-M, Huang Q, Zh-b L, Zhang L-H, Zheng Z-Y, Lin C-Q. Design of highly sensitive phosphorescence sensor for determination of procaterol hydrochloride based on inhibition of $KClO_3$ oxidation fluorescein isothiocyanate. Luminescence 2015;30:382–7.
20. Alarfaj NA, Aly FA, El-Tohamy MF. Application of silver nanoparticles to the chemiluminescence determination of cefditoren pivoxil using the luminol–ferricyanide system. Luminescence 2015;30:91–7.
21. Abdoon FM, Khaleel AI, El-Tohamy MF. Utility of electrochemical sensors for direct determination of nicotinamide (B_3): comparative studies using modified carbon nanotubes and modified β-cyclodextrin sensors. Sens Lett 2015;13:462–70.
22. Lyon AW, Meinert P, Bruce GA, Laxdal VA, Salkie ML. Influence of methodology on the detection and diagnosis of congenital analbuminemia. Clin Chem 1998;44:2365–7.
23. Shahabadi N, Maghsudi M, Nemati L. Design of green magneto-fluorescent γ-Fe_2O_3–methyldopa conjugate nanocrystal as a targeted probe for monitoring of esterase activity. J Photochem Photobiol B 2015;149:215–23.
24. Sen T, Haldar KK, Patra A. Au nanoparticle-based surface energy transfer probe for conformational changes of BSA protein. J Phys Chem C 2008;112:17945−51.
25. Asha Jhonsi M, Kathiravan A, Renganathan R. Spectroscopic studies on the interaction of colloidal capped CdS nanoparticles with bovine serum albumin. Colloid Surf B 2009;72:167−72.
26. Iosin M, Toderas F, Baldeck PL, Astilean S. Study of protein–gold nanoparticle conjugates by fluorescence and surface-enhanced Raman scattering. J Mol Struct 2009;924–6:196–200.
27. Lakowicz JR. *Principles of Fluorescence Spectroscopy*. 3rd ed. Springer Science: New York, 2006.
28. Thipperudrappa J, Biradar DS, Lagare MT, Hanagodimath SM, Inamdar SR, Kadadevaramath JS. Fluorescence quenching of BPBD by aniline in benzene–acetonitrile mixtures. J Photochem Photobiol A 2006;177:89–93.
29. Huang CY. Determination of binding stoichiometry by the continuous variation method: the Job plot. Methods Enzymol 1982;87:509–25.
30. Selley ML, Madsen BW, Thomas J. Protein binding of tolmetin. Clin Pharmacol Ther 1978;24:694–705.
31. Matsuyama K, Sen AC, Perrin JH. The effects of pH, calcium and chloride ions on the binding of tolmetin to human serum albumin: circular dichroic, dialysis and fluorometric measurements. J Pharm Pharmacol 1978;39:190–5.
32. Wei XL, Xiao JB, Wang Y, Bai Y. Which model based on fluorescence quenching is suitable to study the interaction between *trans*-resveratrol and BSA? Spectrochim Acta A 2010;75:299–304.
33. van de Weert M, Stella L. Fluorescence quenching and ligand binding: a critical discussion of a popular methodology. J Mol Struct 2011;998:144–50.
34. Ross PD, Subramanian S. Thermodynamics of protein association reactions: forces contributing to stability. Biochemistry 1981;20:3096–102.
35. Varshney A, Rehan M, Subbarao N, Rabbani G, Khan RH. Elimination of endogenous toxin, creatinine from blood plasma depends on albumin conformation: site specific uremic toxicity and impaired drug binding. PLoS One 2011;6:e17230.
36. Sen T, Haldar KK, Patra A. Au nanoparticle-based surface energy transfer probe for conformational changes of BSA protein. J Phys Chem C 2008;112:17945–51.
37. Mohammed A, Gray HB, Weaver JJ, Sarasaenee K, Gross Z. Amphiphilic corroles bind tightly to human serum albumin. Bioconjugate Chem 2004;15:738–46.
38. Foster T. Intermolecular energy hike and fluorescence. Ann Phys 1948;2:55–75.
39. Rowel HM, Meidtner K, Kroll J. Binding of selected phenolic compounds to proteins J Agri Food Chem 2005;53:4228–35.
40. Shahabadi N, Maghsudi M. Binding studies of a new copper (II) complex containing mixed aliphatic and aromatic dinitrogen ligands with bovine serum albumin using different instrumental methods. J Mol Struct 2009;92:193–9.